ACS Sustainable Chemistry & Engineering

Research Article

Cite This: ACS Sustainable Chem. Eng. 2019, 7, 7353−7361

pubs.acs.org/journal/ascecg

Thioether-Functionalized Covalent Triazine Nanospheres: A Robust Adsorbent for Mercury Removal

Sujan Mondal,[†] Sauvik Chatterjee,[†] Saptarsi Mondal,[‡] and Asim Bhaumik*[,†]

[†]School of Materials Science and [‡]School of Chemical Sciences, Indian Association for the Cultivation of Science, 2A & B, Raja S. C. Mullick Road, Jadavpur, Kolkata−700032, India

Supporting Information

ABSTRACT: Hg/Hg(II) have been recognized as being highly poisonous to humans as they cause severe health and environmental problems. Designing a suitable adsorbent decorated with an abundance of accessible chelating sites at the solid surface together with high affinity for heavy metals is a big challenge to overcoming mercury contamination. Here we report a new thioether-functionalized covalent triazine nanosphere, SCTN-1, which has been employed as a highly efficient adsorbent for the removal of toxic mercury from contaminated water with an excellent adsorption performance of 1253 and 813 mg g^{-1} for Hg^{2+} and Hg(0) respectively, which largely outperforms several recently reported thiol and thioether-functionalized adsorbents. Our kinetic studies suggest that SCTN-1 showed the fastest adsorption rate for the removal of mercury from aqueous solutions among all adsorbents known until date. Based on its adsorption performance and high recycling efficiency, this thio-functionalized nanoporous polymeric material has huge potential to be explored in environmental remediation.

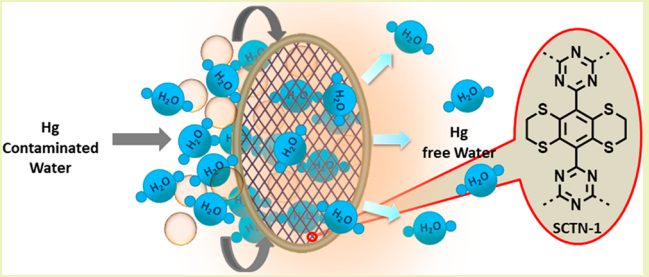

KEYWORDS: *Microporous materials, Covalent triazine networks, Thioether functionalized material, Mercury removal, Recyclable adsorbent*

INTRODUCTION

Mercury (Hg) pollution is a serious threat to our health and environment.[1,2] Exposure to mercury poisoning often results a wide range of severe life threatening diseases.[3,4] Hg/Hg(II) can be released by both natural and anthropogenic processes.[5] The major contamination of mercury comes from sources like drinking water or via crops from irrigation water, which comes from human activities including a variety of industrial processes, oil and coal burning, mining of mercury ores, use of mercury in products and manufacturing, cement production, etc. The toxicity level of mercury largely depends on its chemical form. Usually, mercury exists in organic, inorganic, and metallic forms. Organic mercury (generally, methylmercury and ethylmercury) is more toxic than other mercury species due to their direct action in the human body.[6] However, inorganic mercury ions are more abundant and can be easily converted to more toxic alkyl mercury species through biological activities.[7] But most of the mercury species present in water exists in the form of Hg^{2+} ions. Therefore, it is very important to remove the Hg^{2+} ion from the contaminated aqueous solutions.

Several strategies have been developed over the years to reduce the concentration of toxic mercury. The popular processes for the Hg(II) removal include complexation by reduced sulfur-containing ligands,[8] membrane filtration,[9] coagulation,[10] adsorption,[11−14] chemical reduction,[15] etc. Compared with other traditional separation technologies, adsorption is considered as the best technique due to the simplicity in setup and cost efficiency. In this respect, porous nanomaterials are very promising candidates. So far, porous nanomaterials copiously employed in gas storage and separation,[16,17] energy storage,[18,19] catalysis,[20−22] and other frontline areas of energy research.[23,24] Owing to their structural diversity, tunable porosity, good surface hydrophobicity, and high accessible specific surface area porous organic materials have a huge scope to be explored as adsorbent. Organic nanoporous materials bearing reactive functional groups can be designed through proper choices of monomeric building blocks. These frameworks contain no heavy metal ions, leading to very low skeletal density. Moreover, they possess the additional advantages of being less sensitive to moisture or air.[25] Although, there are reports of sulfur-containing porous adsorbents for mercury removal,[26,27] they have their own limitations. For example MP-HMS, a silica based functional porous material[28] suffers from the problem of durability as an adsorbent due to hydrolysis in the long run. Thus, we have focused our interest to design an organic porous nanostructured material as adsorbent with high adsorption capacity, easy separation, and regeneration efficiency. Today, a wide variety of adsorbent materials including organic polymers,[29,30]

Received: January 28, 2019
Revised: February 27, 2019
Published: March 11, 2019

DOI: 10.1021/acssuschemeng.9b00567
ACS Sustainable Chem. Eng. 2019, 7, 7353−7361

Scheme 1. Synthesis of Thioether-Based Covalent Triazine Nanosphere (SCTN-1)

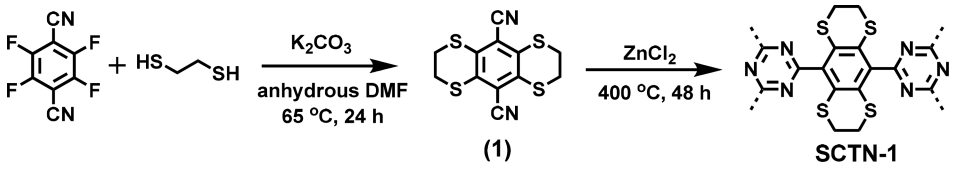

porous silica,[31,32] nanoparticles,[33,34] hydrogels,[35,36] graphene composite,[37,38] metal−organic frameworks (MOFs),[39,40] polypyrrole-MoS_4,[41] etc., have been designed and tested for the possible removal of mercury. However, with difficulties like complex route in material synthesis or limitations in reusability, pH sensitivity, etc., designing more efficient material for mercury removal under optimal conditions is an area of continuous research interest. Surface modified adsorbent bearing heteroatoms have shown good binding affinity toward heavy metal ions.[42,43] Sulfur and mercury, being a soft base and soft acid, respectively, bind very easily and give a very high adsorption rate.[44−46] Due to exceptionally high BET surface area and excellent chemical and thermal stability, covalent triazine frameworks (CTFs)[47−49] have huge potential to be explored as the adsorbent in this context. Further, ease of fabrication of sulfur containing functional groups in the organic backbone in the form of thiol, thiourea, or thioether, can make the porous organic nanomaterials ideal adsorbents for mercury removal application. The reusability, adsorption rate, and kinetics can be improved through numerous modifications in the porous organic network via novel synthetic routes and functionalization strategies. Conventionally, only S−Hg interaction has been discussed to tune mercury adsorption capacity. A cooperative role of hard and soft center by exploring the capacity of mercury adsorption using N and S centers at a time can give a new insight in this field.

Herein, we proposed a strategy for designing a covalent triazine nanosphere (SCTN-1) with dense and flexible thioether chelating arms (Scheme 1). To build the porous networks we have employed an ionothermal approach using $ZnCl_2$ as catalyst. The resulting rigid microporous triazine networks exhibited considerably high BET surface area (1459 $m^2\ g^{-1}$) with high thermal stability and it showed significant application for the selective detection and quick removal of toxic Hg^{2+}. Detailed adsorption studies and kinetics over the newly developed porous adsorbent SCTN-1 have been systematically investigated and results offer a new inspiration for the development of efficient adsorbents for environmental applications. Further, density functional theory (DFT) has been employed to understand the interaction of mercury with SCTN-1 and it offers a new scope of development of materials containing both hard and soft Lewis basic centers for effective adsorption and removal of mercury from contaminated water.

EXPERIMENTAL SECTION

Materials. Tetrafluoroterephthalonitrile and 1,2-ethanedithiol were purchased from Sigma-Aldrich. Potassium carbonate, anhydrous $ZnCl_2$, and anhydrous DMF were received from Spectrochem, India. Other solvents and acids were supplied from a local commercial source. All the chemicals were used without further purification. Deionized water was used throughout the experiment.

Instrumentation. ^{1}H NMR spectrum of the monomer was recorded on Bruker Advance 400 MHz NMR spectrometer. Powder X-ray diffraction (PXRD) patterns were recorded with a Bruker D8 Advance X-ray diffractometer using Ni-filtered Cu Kα (λ = 0.15406 nm) radiation. Elemental analyses (C, H, N, and S) were performed on a PerkinElmer 2400 series-II CHN analyzer. Thermogravimetry (TG) measurement was carried out using a thermal analyzer TA-SDT Q-600 under compressed air flow with heating rate 10 °C/min. Nitrogen adsorption/desorption measurement was performed with an Autosorb-iQ surface analyzer (Quantachrome Instruments, USA) at 77 K. Prior to the measurement, the sample was degassed in vacuum at 150 °C for 6 h to remove all the guests present in material. The specific surface area was estimated by using Brunauer−Emmett−Teller (BET) model. The pore size distributions of SCTN-1 was derived by the nonlocal density functional theory (NLDFT) method from adsorption branch of the isotherm. IR spectrum was recorded on ATR mode by using Shimadzu FTIR Spectrometer. Solid-state ^{13}C CP-MAS NMR study was performed using a Bruker Advanced II spectrometer at 500 MHz with a MAS frequency of 8 kHz. Ultra-High resolution transmission electron microscopic (FEG-TEM) images were recorded in a JEOL JEM 2010 transmission electron microscope with operating voltage 200 kV equipped with a FEG. X-ray photoelectron spectroscopy (XPS) was performed on an Omicron Nanotech operated at 15 kV and 20 mA. The quantitative analyses of metal ions were carried out in a PerkinElmer Optima 2100 DV ICP-OES instrument.

General Procedure for Thioether-Based Ligand (1). A two-neck round-bottom flask was charged with tetrafluoroterephthalonitrile (1.0 g, 5 mmol), 1,2-ethanedithiol (1.034g, 11.5 mmol), and potassium carbonate (4.7 g, 34.5 mmol) along with 35 mL of anhydrous DMF under an inert atmosphere of nitrogen. Then, the reaction mixture was heated at 65 °C temperature under stirring for 24 h. After cooling to room temperature, the yellow precipitate was filtered and the solid was washed thoroughly with water and acetone. The final solid was air-dried to obtain 85% pure product. ^{1}H NMR (400 MHz, $CDCl_3$) δ = 3.4 (s, 8 H); ^{13}C NMR (100 MHz, $CDCl_3$/DMSO-d^6) δ = 134.17, 113.21, 112.55, 28.43.

General Procedure for SCTN-1. In a typical synthesis of SCTN-1, a quartz tube was first charged with thio-ether ligand (**1**) (200 mg, 5.2 mmol) and anhydrous $ZnCl_2$ (5 equiv). The tube was flame-sealed under vacuum and placed into an oven. Then the system was heated to 400 °C for 48 h. After cooling to ambient temperature the tube was opened and the content was ground to a fine powder. The crude product was washed with plenty of water and then the product was stirred in 1 M HCl for 10 h and filtered. Finally, the product was subsequently washed with water, THF, and dried overnight under vacuum. Further, Soxhlet extraction has been carried out on SCTN-1 in methanol to make it free from adsorbed solvents and monomers.

Hg^{2+} Adsorption Kinetics. To choose the dosage amount of the adsorbent we first used three different dosages. We used 10, 15, and 20 mg of SCTN-1 in 25 mL 5 ppm mercury solutions. We found that with 10 mg SCTN-1 the concentration of the final solution was 9.2 ppb, whereas with 15 and 20 mg dosage the concentration was well below 2 ppb limit. As there was no significant improvement of mercury removal upon increase in the dosage, in a typical experiment 15 mg of adsorbent SCTN-1was dispersed in 25 mL of Hg^{2+} aqueous solution with a predefined initial concentration. The mixture was then stirred at room temperature for 2 h. After appropriate time intervals, 2 mL of aliquots were withdrawn immediately from the system. The treated solutions were then filtrated followed by centrifugation. The resulting Hg^{2+} concentrations in the supernatant liquids were analyzed using ICP-OES.

The removal efficiency of Hg^{2+} at different time interval was calculated as follows:

DOI: 10.1021/acssuschemeng.9b00567
ACS Sustainable Chem. Eng. 2019, 7, 7353−7361

$$R(\%) = \frac{C_0 - C_t}{C_0} \times 100$$

Where R (%) denotes the removal efficiency of Hg^{2+}, C_0 (mg/L) is the initial Hg^{2+} concentration in the system, and C_t (mg/L) is the Hg^{2+} concentration in solution at time t (min).

Selectivity Tests. To a 200 mL aqueous solution of $Hg(NO_3)_2$, $Cu(NO_3)_2$, $Zn(NO_3)_2$, $Mg(NO_3)_2$, $Cd(NO_3)_2$, $Pb(NO_3)_2$, $Co(NO_3)_2$, $NaNO_3$, and KNO_3 in an Erlenmeyer flask 50 mg of SCTN-1 was added. The mixture was then stirred at room temperature and after appropriate time intervals, 50 mL of aliquots were taken out from the system. The adsorbents were removed by filtration followed by centrifugation. Finally, the concentration of different ions in those solution were analyzed by ICP-OES.

Hg^{2+} Adsorption Isotherm. To a 50 mL aqueous solutions of Hg(II) with different concentration, 10 mg of adsorbent SCTN-1 was added and stirred at room temperature. This was followed by sonication for 12 h to confirm complete adsorption has taken place by this time. The mixture was then centrifuged and filtered to get supernatant solution. Finally the supernatant was analyzed by ICP-OES.

Determination of q_t and q_e. The adsorbed amount of mercury at time t (δ_t, mg g^{-1}) was calculated by the equation:

$$q_t = (C_0 - C_t)\frac{V}{m}$$

Where C_0 is the initial concentration of the Hg^{2+} in the solution, C_t is the concentration of the Hg^{2+} in the solution at time t, V is the volume of the solution used for the adsorption experiment, and m is the mass of the adsorbent used.

The value of q_e is calculated from the intercept of eq 1.

Mercury Vapor Capture Experiments. A small glass vial containing 350 mg elemental mercury was placed into a 20 mL vial with 25 mg of adsorbent SCTN-1. Then the full system was placed into an autoclave and kept in an oven at 150 °C for 72 h. After cooling to room temperature, the adsorbent was collected. The weight gained after mercury adsorption was measured to evaluate the amount of mercury captured during the experiment. ICP analysis was carried out to prove the presence of mercury inside the adsorbent. A 5 mg portion of elemental mercury adsorbed adsorbent was dissolved in 5 mL of aqua regia, and then, it was diluted with distilled water to make the stock solution for ICP-OES analysis.

RESULTS AND DISCUSSION

Powder X-ray diffraction (PXRD) patterns of SCTN-1 (Figure S1) indicate that the samples are mostly amorphous in nature. A broad diffraction peak located at $2\theta = 25.3°$ corresponding to 001 reflection points to a potential stacking of triazine networks.[50] Detailed information about the chemical composition is obtained through elemental analysis. However, it is pertinent to mention that the experimental result (C, 40.37; H, 4.63; N, 4.71; S, 28.41) revealed some considerable deviation from the calculated theoretical value (C, 46.72; H, 2.61; N, 9.08, S, 41.58). This phenomenon is likely to be due to the decomposition of nitrile groups along with partial carbonization of networks.[51−53]

Further, the chemical environment of different carbon atoms present in the SCTN-1 material is analyzed by the ^{13}C CP-MAS MNR spectrum (Figure 1a). A signal at 28.53 ppm is ascribed to sp^3-hybridized $-CH_2$ carbons of the dithiol moiety. The peak at about 176.84 ppm is observed, which could be attributed to the existence of triazine units in the material. An obvious sharp and intense peak at 140.88 ppm is attributed to the aromatic carbons connected with the sulfur atoms. A shoulder in the signal at 151.89 ppm is observed, which could be attributed to aromatic sp^2 carbons connected by triazine ring. A strong absorption band in the IR spectrum (Figure S2)

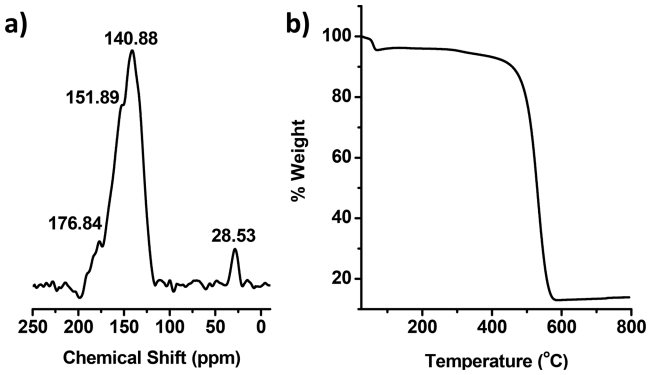

Figure 1. ^{13}C CP-MAS NMR spectrum (a) and thermogravimetric plot (b) of SCTN-1.

at 1366 cm^{-1} suggests the presence of triazine ring to the polymer backbone. The formation of the triazine framework structure is further confirmed from the XPS analysis. The deconvoluted N 1s spectrum (Figure S3) for SCTN-1 shows two peaks with the binding energies of 398.2 and 400.3 eV corresponding to the nitrogen atom of triazine rings.[54,55] In postadsorbed SCTN-1 materials we do not observe any significant change in framework stretching vibrations (Figure S2) as the mercury adsorption proceeds through a noncovalent interaction with the nitrogen and sulfur atoms present in the framework backbone. To evaluate the thermal stability, thermogravimetric analysis (TGA) is conducted under aerobic environment in the temperature range of 25−800 °C. As shown in Figure 1b, the weight loss below 100 °C can be assigned to the evaporation of absorbed water molecule. Then with the continuous increase of temperature, the material is found to be thermally stable up to 453 °C. After that, the process is associated with the decomposition of aromatic rings and other organics present in the materials.

The surface area and porosity of SCTN-1 is estimated by N_2 adsorption analysis at 77 K. As shown in Figure 2, SCTN-1

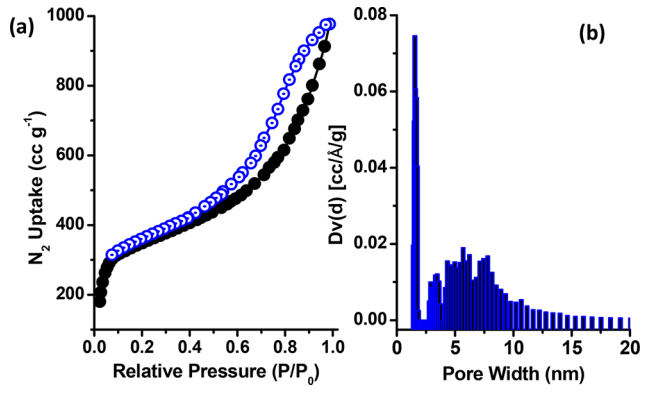

Figure 2. Nitrogen adsorption/desorption isotherm (a) and respective pore size distribution plot employing NLDFT method (b) for SCTN-1 at 77 K.

exhibits a combination of type I and type IV isotherms, representing the presence of well-developed micropores. The isotherm displays a rapid nitrogen uptake at lower relative pressure ($P/P_0 < 0.02$) followed by a gradual increase in adsorption at higher P/P_0 values, which can be ascribed to the coexistence of micropores and broad mesopores. The nitrogen adsorption isotherm reveals that the SCTN-1 has a highly

DOI: 10.1021/acssuschemeng.9b00567
ACS Sustainable Chem. Eng. 2019, 7, 7353−7361

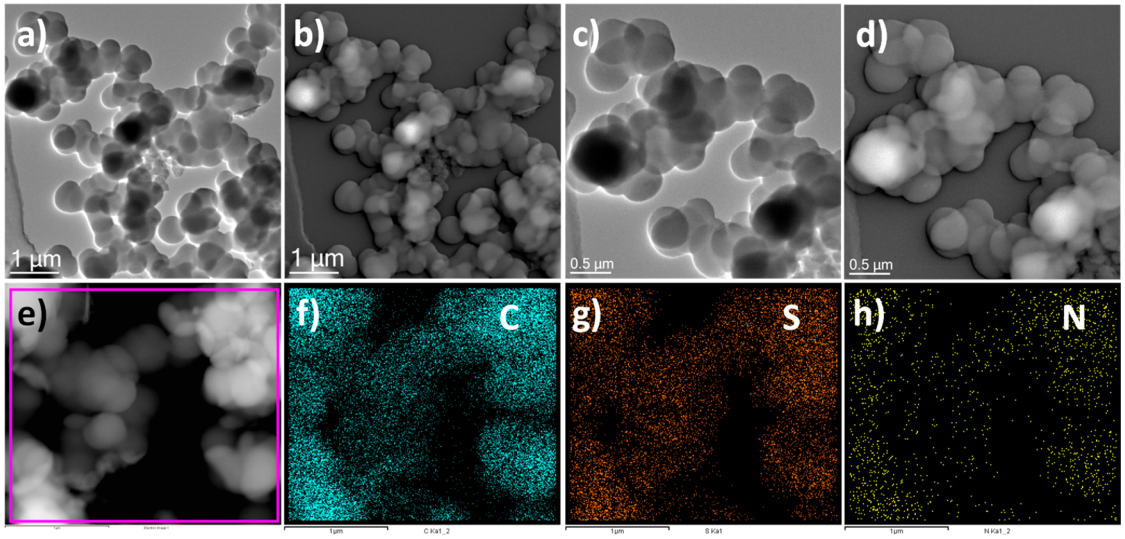

Figure 3. HRTEM images (a–d) with reverse phase contrast (b and d) for SCTN-1 nanosphere. Scanning TEM elemental mapping of C, S, and N elements (e–h) for SCTN-1.

porous structure with a BET surface area of 1459 $m^2\ g^{-1}$ and high micropore volume (1.52 $cm^3\ g^{-1}$). SCTN-1 showed pores significantly located in the micropore region, below 2 nm. Further, SCTN-1 exhibited large desorption hysteresis, which could be attributed to wider pores in the range of 3.0–9.0 nm, suggesting the presence of bimodal micro- and mesoporosity (Figure 2b). Transmission electron microscopic (TEM) images of the representative thioether-based SCTN-1 material are shown in Figure 3a–d. These TEM images reveal that the SCTN-1 material is composed of uniform and homogeneously distributed nanospheres of dimension 450–550 nm. To elucidate further, elemental mapping is performed to analyze the elemental distribution in SCTN-1 material. From the mapping images (Figure 3e–h) it is evident that the elements C, N, and S are homogeneously distributed in the materials.

To gain further information about the remarkable binding interaction between mercury and our adsorbent, SCTN-1 is analyzed through XPS. As seen from Figure 4a, after mercury

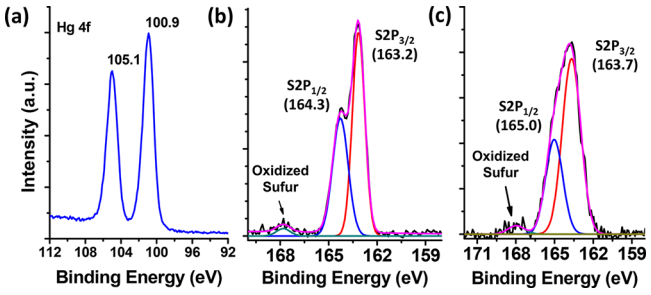

Figure 4. High-resolution XPS spectra of (a) Hg 4f, (b) S 2p (before mercury adsorption), and (c) S 2p (after mercury adsorption).

adsorption, the binding energy of the Hg 4f region appears at 100.9 and 105.1 eV, corresponding to Hg $4f_{7/2}$ and Hg $4f_{5/2}$ signals, respectively.[30,56] A strong S 2p signal (Figure 4) is observed for SCTN-1 materials with S $2p_{3/2}$ and $2p_{1/2}$ doublet at 163.2 and 164.3 eV. In postadsorbed material, the binding energy of the S 2p peak shifts toward higher binding energy value, which could be attributed to strong coordination of electron-rich sulfur with mercury. On the contrary, the N 1s peaks of SCTN-1 (Figure S3) exhibit a positive shift by 0.5 eV upon adsorption of Hg^{2+}, indicating the chelating interaction between nitrogen and Hg^{2+}. Based on the XPS survey spectra, it is clear that Hg^{2+} adsorption likely takes place by developing an interaction with the sulfur and nitrogen atoms of SCTN-1.

The world health organization (WHO) sets the permissible limit for mercury in drinking water to be 2 ppb. Thus, providing mercury-free drinking water to the masses is a big challenge. Being a material consisting of a thioether moiety, SCTN-1 is investigated for Hg(II) removal efficiency from water. The soft–soft interaction between mercury and thioether leads to excellent adsorption and retention capacity of Hg(II) and can be easily removed to regenerate the material for further use by treatment with dilute HCl for 15 min followed by filtration. The material has a high BET surface area, and it shows very high efficiency for Hg(II) adsorption at par with expectation. The adsorption isotherm is matched with the Langmuir model which fits well with an R^2 value >0.999. SCTN-1 shows a mercury removal capacity of 1253 mg g^{-1} (Figure 5c) which is better than most of the reported porous organic materials. Comparative data of maximum Hg(II) uptake with some other materials are shown in Table 1. The Jiang group reported TAPB-BMTTPA-COF[56] with an Hg^{2+} adsorption capacity of 734 mg g^{-1}, which was less than our SCTN material. Later, Sun et al. reported COF-S-SH,[30] a covalent organic framework, to show Hg^{2+} ion adsorptions as high as 1350 mg g^{-1}. From the adsorption isotherm, it is quite evident that the adsorption time is very low for Hg(II), which makes it very good for real time application for mercury removal from contaminated groundwater. The concentration of the Hg(II) contaminated solution with 5 ppm drops down to 1.6 ppb, which is permissible by WHO within just 5 min of initiation (Figure 5a and b). This clarifies 99.99% (R%) of mercury from the solution was removed from the solution within 5 min of contact time. The adsorption kinetics was well matched with the pseudo-second-order kinetics model for adsorption proposed by Ho and McKay (eq 1).[57]

$$\frac{t}{q_t} = \frac{1}{k_2 q_e^2} + \frac{t}{q_e} \qquad (1)$$

Where, k_2 is the adsorption rate constant (g mg^{-1} min^{-1}), and q_t and q_e are the Hg^{2+} uptake capacities (mg g^{-1}) at time t

DOI: 10.1021/acssuschemeng.9b00567
ACS Sustainable Chem. Eng. 2019, 7, 7353–7361

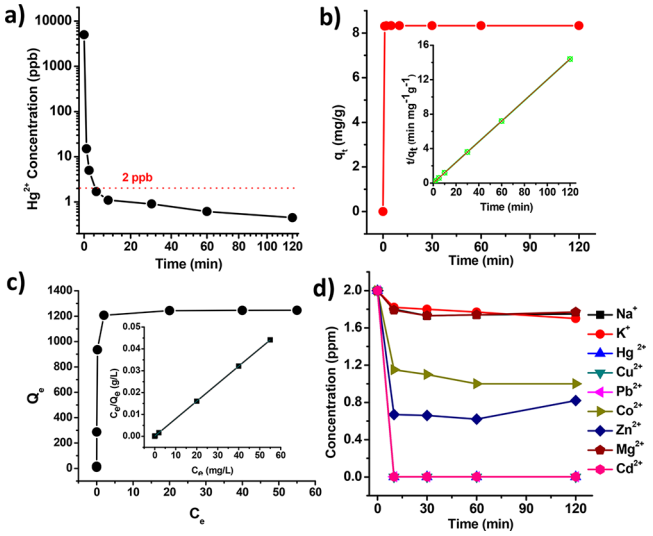

Figure 5. (a) Hg(II) sorption kinetics with the initial Hg(II) concentration of 5 ppm. (b) Hg(II) adsorption versus contact time in aqueous solution for 5 ppm. Pseudo-second-order kinetic plot for the adsorption at Hg(II) concentration of 5 ppm is shown in the inset. (c) Hg(II) uptake isotherm after 12 h. The linear regression by fitting the equilibrium data with the Langmuir model is shown in the inset. (d) Hg(II) capture efficiency in removing metal ions by SCTN-1.

Table 1. Comparison of Hg^{2+} Uptake Amount and K_d Value for SCTN-1 with Those of Other Benchmark Porous Materials

		maximum mercury uptake (mg g^{-1})			
entry	porous materials	Hg(II)	Hg(0)	distribution coefficient, K_d (mL g^{-1})	ref
1	POP-SH	1216	630	5.5×10^8	29
2	COF-S-SH	1350	863	2.3×10^9	30
3	PANI/RGO	1000			38
4	TAPB-BMTTPA-COF	734		7.82×10^5	56
5	nanoselenium sponge	324		1.67×10^9	58
6	MNPCs	476			59
7	PAF-1-SH	1000		5.76×10^7	60
8	Zr-DMBD	171.5		9.99×10^5	61
9	LHMS-1			6.4×10^6	62
10	**SCTN-1**	**1253**	**813**	**1.89×10^8**	**this work**

(min) and equilibrium, respectively. The rate constant (k_2) value is found to be 55 g mg^{-1} min^{-1}, and the correlation coefficient value (>0.999) is very high, indicating a good fit with pseudo-second-order kinetics (Figure 5b). The high k_2 value also indicate fastest uptake kinetics reported until date, which is almost 9 times faster than that of TAPB-BMTTPA-COF and 7 times than PAF-1-SH. A possible reason for this fast kinetics is the very high accessible surface area and pore volume of SCTN-1 together with surface bound thioether moieties. In 2 h the concentration of Hg(II) reaches 0.4 ppb. The value of the affinity of the absorbent toward mercury, distribution coefficient (K_d), was thus analyzed by the given eq 2.

$$K_d = \frac{C_0 - C_e}{C_e} \times \frac{V}{m} \quad (2)$$

Where C_0 and C_e are the initial and equilibrium concentrations of Hg^{2+}, V is the volume of solution (mL), and m is the amount of adsorbent taken (g). The K_d for SCTN-1 was found to be 1.89×10^8 mL g^{-1} which is quite higher than the most commercially popular and benchmark materials, which have lower K_d values as presented in Table 1.

Mercury vapor absorption capacity is one of the most interesting properties for detoxification application in the flue gas industry. It requires high uptake of mercury in metallic state at very high temperature. We have measured the mercury vapor uptake capability at 150 °C and found to be 813 mg g^{-1}, which is only the second best reported Hg(0) uptake capacity until date after COF-S-SH (865 mg g^{-1}). Even commercially used materials like activated carbon have a mercury vapor absorption capacity of 47 mg g^{-1}, although it has a BET surface area as high as 1011 m^2 g^{-1}.

To get an idea about the mechanism of adsorption kinetics, the data points are fitted with the Weber and Morris intraparticle diffusion model.[63] From the plotted data (q_t versus $t^{1/2}$) according to eq 3, we find a linear plot almost parallel to the time axis (Figure S7) indicating micropore diffusion, which is expected from SCTN-1 as this material showed uniform pore size distribution in the micropore region.[64] The high intercept value is indicative of the boundary layer thickness.

$$q_t = k_{id}(t^{1/2}) + C \quad (3)$$

Where k_{id} (mg g^{-1} $min^{-1/2}$) is the intraparticle diffusion rate parameter and C (mg g^{-1}) is a constant related to boundary layer thickness.

To understand how the material could abstract Hg^{2+}, we consider a model system, which is the repetitive unit of the ligand. To understand how Hg^{2+} binds to the ligand we study the 1:1 (COMP11), 1:2 (COMP12), 1:3 (COMP13), and 1:4 (COMP14) complex of the Hg^{2+} and the ligand. We optimize all the complexes using B3LYP density functional and calculate their zero-point vibrational energy (ZPVE) corrected stabilization energy (Table S1). All the optimized geometries of the complexes along with their stabilization energies are shown in Figure S8. We plot the stabilization energy of the complexes with respect to the number of Hg^{2+} in Figure 6a. The stabilization energy of COMP11 and COMP12 are −213.6 and −195.7 kcal mol^{-1}, respectively, whereas they are +45.7 and +498.2 kcal mol^{-1} for COMP13 and COMP14, respectively. This indicates that the ligand studied can easily bind up to two Hg^{2+} through $Hg^{2+}\cdots S$ and $Hg^{2+}\cdots N$ strong noncovalent interactions.

To understand the bonding nature of different noncovalent interactions present in the COMP12 complex we further generate a molecular density map and calculate the electron density (ρ) and Laplacian of electron density ($\nabla^2\rho$) using AIM software at different bond critical points (BCPs). The ρ and $\nabla^2\rho$ for the $Hg^{2+}\cdots S$ interaction in COMP12 is found to be 0.055 and 0.174, respectively, whereas for the $Hg^{2+}\cdots N$ interactions, they are 0.036 and 0.083, respectively, at the BCPs. The electron density map of the COMP12 complex is shown in Figure 6b, and the values of ρ and $\nabla^2\rho$ for all kind of interactions in the complex are tabulated in Table 2. The presence of the (3, −1) BCP along with the higher and positive

DOI: 10.1021/acssuschemeng.9b00567
ACS Sustainable Chem. Eng. 2019, 7, 7353−7361

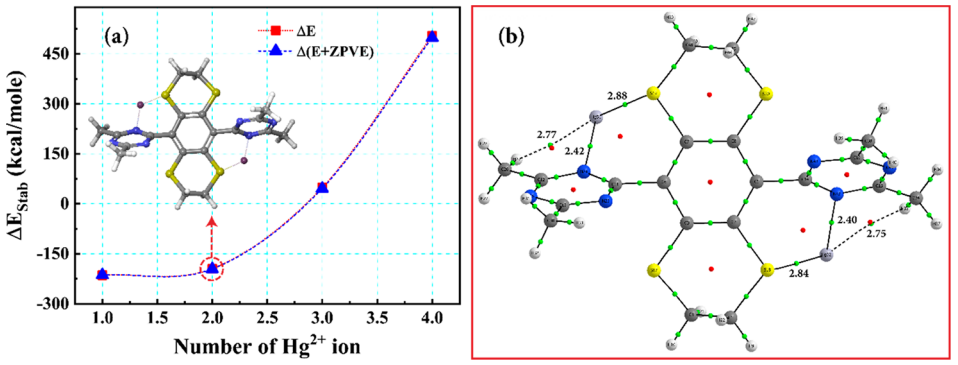

Figure 6. Plot of the stabilization energy of the complex between Hg^{2+} and the ligand with respect to the number of Hg^{2+} ions (a). The stabilization energy for the COMP13 and COMP14 complexes are hugely positive which indicates that the ligand can bind up to two Hg^{2+}. The optimized geometry of the COMP12 complex has also been shown in the plot for clarity. The spheres in white, yellow, gray, blue, and violet color are H, S, C, N, and Hg, respectively. The electron density map of the COMP12 has been shown (b) where green spheres indicate the bond critical point (BCP) and the red spheres indicate the ring critical point (RCP). The distance between two interacting atoms has been shown in angstroms. The presence of very strong $Hg^{2+}\cdots$S and $Hg^{2+}\cdots$N interactions explains the very high stabilization energy.

Table 2. List of Stabilization Energy (ΔE_{stab}, kcal/mol) of the COMP12, Electron Density (ρ, au), Laplacian of Electron Density ($\nabla^2\rho$, au), and Ellipticity (ε) at the BCPs of the Different Noncovalent Interaction in the COMP12 Calculated at B3LYP/6-31+G(d,p);LanL2DZ(Hg) Level of Theory

interaction (COMP12)	ΔE_{Stab}^{ZPE} (kcal/mol)	ρ	$\nabla^2\rho$	ε	distance (Å)	type of interaction
$Hg^{2+}\cdots$N	−195.7	0.055	0.174	0.062	2.42	very strong
		0.053	0.166	0.063	2.40	
$Hg^{2+}\cdots$S		0.036	0.083	0.065	2.88	very strong
		0.033	0.077	0.080	2.84	
$Hg^{2+}\cdots$H—C		0.011	0.035	2.175	2.77	very weak
		0.010	0.034	4.420	2.75	

value of ρ and $\nabla^2\rho$ for the $Hg^{2+}\cdots$S/N interaction indicate that the Hg^{2+} strongly interacts with N and S lone pairs and explains the enormous stabilization energy of the complex. Surprisingly, we have also found the existence of very weak $Hg^{2+}\cdots$H—C interactions where ρ and $\nabla^2\rho$ values are 0.011 and 0.035, respectively. The ellipticity (ε) at the BCPs of $Hg^{2+}\cdots$S/N COMP12 is tabulated in Table 2 as well. The ellipticity measures the anisotropy of the curvature of the electron density at a particular BCP. The greater the values of ε, the greater is the accumulation of the electron density at the perpendicular direction of the interacting plane at that BCP and the greater is the π character of that bond. The ε values for the $Hg^{2+}\cdots$N and $Hg^{2+}\cdots$S interactions are 0.062 and 0.065 which are very low. These low values of ε indicate that the interactions are powerful and have profound σ bond character. On the other hand, a high ε value, 2.175, for $Hg^{2+}\cdots$H—C interaction suggests that the interaction is very weak and has significant π bond contribution.

To investigate the influence of pH, mercury adsorption experiments are carried out under different pH conditions (pH 2−10). The experimental results (Figure S9) show that the mercury adsorption efficiency of SCTN-1 is decreased to some extent at lower pH, retaining its removal efficiency at pH 6 or above. In acidic pH solution, the nitrogen atom of the triazine ring gets protonated and thus the adsorption discrepancy is observed. When the experiments were carried out at different temperatures the results (Figure S10) were found good for real time applications. At 10 °C and room temperature, the results were exactly same. The adsorption decreased slightly when the experiments were carried out at 50 °C. However, the adsorption of mercury is found to be sufficiently low when the experiment temperature was 80 °C which is possibly due to the fact that at higher temperature the adsorbed mercury leaches out back to the solution over time.

The effect of natural organic matters (NOMs) in water during mercury adsorption at room temperature is checked. For that purpose pond water with a good aquatic ecosystem and a water sample collected from the Bay of Bengal are used to prepare the standard mercury solutions. The result shows no significant change in the activity of mercury adsorption in the presence of NOMs. In both cases the mercury concentration reaches below 0.5 ppb with the removal efficiency of 99.99% and K_d of the order 1.78×10^8 mL g^{-1}.

The selectivity of the material toward different ions has been tested using a solution prepared with eight different metal cations with 2 ppm concentration each and analyzed in ICP-OES. The high selectivity is observed for Hg^{2+} ion in the presence of other cations like K^+, Na^+, Zn^{2+}, Co^{2+}, Cr^{2+}, and Mg^{2+}. Only exceptions being Cd^{2+}, Cu^{2+}, and Pb^{2+} concentrations of which are reduced below 2 ppb level after 2 h of contact to the material. The removal efficiency (R%) for Cd^{2+}, Pb^{2+}, and Cu^{2+} are found to be >99% along with Hg^{2+} for SCTN-1 in 2 h (Figure 5d). This is an attribute of the soft−soft interaction between the sulfur center and the metal ions. The relatively hard metal ions are reluctant toward adsorption. Hence, this S-rich covalent triazine network displays high efficiency for the removal of heavy metal ions.

The SCTN-1 material is employed as adsorbent for seven consecutive cycles to explore its potential in sustainable operation. For that purpose the material is collected after the first cycle of removal and stirred with 25 mL 6.0 M HCl for 2

DOI: 10.1021/acssuschemeng.9b00567
ACS Sustainable Chem. Eng. 2019, 7, 7353−7361

h. After washing with 100 mL water dried in an oven overnight, the material SCTN-1 is then reused to remove mercury and it is found to be as competent as it was in the first cycle up to the seventh cycle. The adsorption efficiencies of SCTN-1 for the removal of Hg(II) from the contaminated stock solutions are presented in Figure 7, for seven consecutive cycles. It is seen

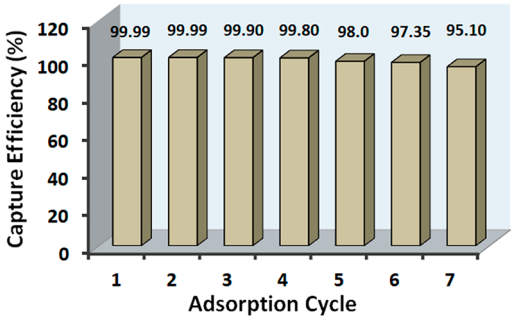

Figure 7. Recyclable performance for Hg(II) removal in aqueous solution.

from this bar diagram that SCTN-1 has retained over 95% Hg(II) removal efficiency in the seventh cycle, suggesting the highly efficient and robust nature of this adsorbent. After the fifth cycle, reused SCTN-1 was further characterized by X-ray and TEM analysis to investigate any noticeable changes during the course of the adsorption study. The X-ray pattern (Figure S11) of the reused adsorbent remains unchanged, which suggests its high mechanical stability. In addition TEM analysis (Figure S12) reveals that the nanosphere morphology is unaltered.

CONCLUSIONS

Thus, our experimental results suggest that a rigid microporous triazine network material high surface area together with densely distributed thioether moiety in the porous framework can be synthesized via an ionothermal approach using $ZnCl_2$ as catalyst. This thioether-functionalized covalent triazine network material shows exceptionally high Hg^{2+} and Hg(0) uptake capacities of 1253 and 813 mg g^{-1}, respectively. We investigated different nonbonding interactions between Hg^{2+} and the ligand using an ab initio quantum chemistry method and AIM analysis to understand why this thioether-functionalized covalent triazine network material shows high efficiency for the Hg^{2+} abstraction. The stabilization energy of the complex suggests that one ligand can efficiently bind up to two Hg^{2+}. The AIM analysis confirms that Hg^{2+} interacts with the N and S lone pair of the ligand very strongly. Along with the stronger $Hg^{2+}\cdots N$ and $Hg^{2+}\cdots S$ interactions, we have also found very weak $Hg^{2+}\cdots H—C$ interaction in the complex studied. Therefore, it can be concluded that the high Hg^{2+} abstraction by the material is the consequence of the several stronger and weaker noncovalent interaction between Hg^{2+} and the ligand. Removal of toxic mercury by this organic porous material is aided by simple operation procedure, very fast adsorption kinetics, and high distribution coefficients together with ease of regeneration of the adsorbent reported; these features reported herein can contribute significantly in the grassroots level application for combating the ordeals of the purified drinking water crisis in the future.

ASSOCIATED CONTENT

Supporting Information

The Supporting Information is available free of charge on the ACS Publications website at DOI: 10.1021/acssuschemeng.9b00567.

Powder X-ray diffraction pattern of SCTN-1, IR spectrum, N 1s XPS spectra of before and after mercury adsorbed material, schematic diagram of mercury [Hg(0)] vapor capture experiment, ^{1}H and ^{13}C NMR spectra of thioether based ligand (**1**), pH and temperature dependence plot, and powder XRD and TEM images of reused SCTN-1 material (PDF)

AUTHOR INFORMATION

Corresponding Author

*E-mail: msab@iacs.res.in.

ORCID

Asim Bhaumik: 0000-0002-4907-7418

Notes

The authors declare no competing financial interest.

ACKNOWLEDGMENTS

S.M. would like thank the CSIR, New Delhi, for his senior research fellowship. S.C. wishes to thank DST, New Delhi, for an INSPIRE fellowship. S.M. would like to thank Dr. Prashant Chandra Singh, Associate Professor, School of Chemical Sciences, Indian Association for the Cultivation of Science, for generously providing the high-end computational facility to carry out theoretical calculations in his cluster. A.B. wishes to thank DST, New Delhi, for an Indo-Egypt international project grant.

REFERENCES

(1) Lubick, N.; Malakoff, D. With Pact's Completion, the Real Work Begins. *Science* **2013**, *341*, 1443−1445.
(2) Li, W. C.; Tse, H. F. Health Risk and Significance of Mercury in the Environment. *Environ. Sci. Pollut. Res.* **2015**, *22*, 192−201.
(3) McNutt, M. Mercury and Health. *Science* **2013**, *341*, 1430.
(4) Li, X.; Bian, C.; Meng, X.; Xiao, F.-S. Design and Synthesis of an Efficient Nanoporous Adsorbent for Hg^{2+} and Pb^{2+} Ions in Water. *J. Mater. Chem. A* **2016**, *4*, 5999−6005.
(5) Wang, Q.; Kim, D.; Dionysiou, D. D.; Sorial, G. A.; Timberlake, D. Sources and Remediation for Mercury Contamination in Aquatic Systems-a Literature Review. *Environ. Pollut.* **2004**, *131*, 323−336.
(6) Luo, F.; Chen, J. L.; Dang, L. D.; Zhou, W. N.; Lin, H. L.; Li, J. Q.; Liu, S. J.; Luo, M. B. High-performance Hg^{2+} Removal from Ultra-low-concentration Aqueous Solution Using Both Acylamide-and Hydroxyl-functionalized Metal-Organic Framework. *J. Mater. Chem. A* **2015**, *3*, 9616−9620.
(7) Maramba, N. P.C.; Reyes, J. P.; Francisco-Rivera, A. T.; Panganiban, L. C.; Dioquino, C.; Dando, N.; Timbang, R.; Akagi, H.; Castillo, M. T.; Quitoriano, C.; Afuang, M.; Matsuyama, A.; Eguchi, T.; Fuchigami, Y. Environmental and Human Exposure Assessment Monitoring of Communities Near an Abandoned Mercury Mine in the Philippines: A Toxic Legacy. *J. Environ. Manage.* **2006**, *81*, 135−145.
(8) Hsu, H.; Sedlak, D. L. Strong Hg(II) Complexation in Municipal Wastewater Effluent and Surface Waters. *Environ. Sci. Technol.* **2003**, *37*, 2743−2749.
(9) Oehmen, A.; Vergel, D.; Fradinho, J.; Reis, M. A. M.; Crespo, J. G.; Velizarov, S. Mercury Removal from Water Streams Through the ion Exchange Membrane Bioreactor Concept. *J. Hazard. Mater.* **2014**, *264*, 65−70.

DOI: 10.1021/acssuschemeng.9b00567
ACS Sustainable Chem. Eng. 2019, 7, 7353−7361

(10) Henneberry, Y. K.; Kraus, T. E. C.; Fleck, J. A.; Krabbenhoft, D. P.; Bachand, P. M.; Horwath, W. R. Removal of Inorganic Mercury and Methylmercury from Surface Waters Following Coagulation of Dissolved Organic Matter with Metal-based Salts. *Sci. Total Environ.* **2011**, *409*, 631−637.
(11) Xu, Y. L.; Zhong, Q.; Liu, X. Y. Elemental mercury oxidation and adsorption on magnesite powder modified by Mn at low temperature. *J. Hazard. Mater.* **2015**, *283*, 252−259.
(12) Jia, F. F.; Wang, Q. M.; Wu, J. S.; Li, Y. M.; Song, S. X. Two-Dimensional Molybdenum Disulfide as a Superb Adsorbent for Removing Hg^{2+} from Water. *ACS Sustainable Chem. Eng.* **2017**, *5*, 7410−7419.
(13) Cao, T. T.; Li, Z.; Xiong, Y.; Yang, Y.; Xu, S. M.; Bisson, T.; Gupta, R.; Xu, Z. H. Silica-Silver Nanocomposites as Regenerable Sorbents for Hg-0 Removal from Flue Gases. *Environ. Sci. Technol.* **2017**, *51*, 11909−11917.
(14) Lisha, K. P.; Maliyekkal, S. M.; Pradeep, T. Manganese dioxide nanowhiskers: A potential adsorbent for the removal of Hg(II) from water. *Chem. Eng. J.* **2010**, *160*, 432−439.
(15) Stolle, R.; Koeser, H.; Gutberlet, H. Oxidation and Reduction of Mercury by SCR DeNOx Catalysts Under Flue Gas Conditions in Coal Fired Power Plants. *Appl. Catal., B* **2014**, *144*, 486−497.
(16) Mondal, S.; Kundu, S. K.; Bhaumik, A. A facile Approach for the Synthesis of Hydroxyl-Rich Microporous Organic Networks for Efficient CO_2 Capture and H_2 Storage. *Chem. Commun.* **2017**, *53*, 2752−2755.
(17) Rieth, A. J.; Dinca, M. Controlled Gas Uptake in Metal-Organic Frameworks with Record Ammonia Sorption. *J. Am. Chem. Soc.* **2018**, *140*, 3461−3466.
(18) DeBlase, C. R.; Silberstein, K. E.; Truong, T.-T.; Abruna, H. D.; Dichtel, W. R. *β*-Ketoenamine-linked Covalent Organic Frameworks Capable of Pseudocapacitive Energy Storage. *J. Am. Chem. Soc.* **2013**, *135*, 16821−16824.
(19) Lee, J. S. M.; Wu, T. H.; Alston, B. M.; Briggs, M. E.; Hasell, T.; Hu, C. C.; Cooper, A. I. Porosity-engineered Carbons for Supercapacitive Energy Storage Using Conjugated Microporous Polymer Precursors. *J. Mater. Chem. A* **2016**, *4*, 7665−7673.
(20) Xu, H.; Gao, J.; Jiang, D. Stable, Crystalline, Porous, Covalent Organic Frameworks as a Platform for Chiral Organocatalysts. *Nat. Chem.* **2015**, *7*, 905−912.
(21) Mondal, S.; Singuru, R.; Shit, S. C.; Hayashi, T.; Irle, S.; Hijikata, Y.; Mondal, J.; Bhaumik, A. Ruthenium Nanoparticle-Decorated Porous Organic Network for Direct Hydrodeoxygenation of Long-Chain Fatty Acids to Alkanes. *ACS Sustainable Chem. Eng.* **2018**, *6*, 1610−1619.
(22) Mondal, S.; Patra, B. C.; Bhaumik, A. One Pot Synthesis of Polyhydroquinoline Derivatives through Organic Solid Acid Catalyzed Hantzsch Condensation Reaction. *ChemCatChem* **2017**, *9*, 1469−1475.
(23) Chandra, S.; Kundu, T.; Dey, K.; Addicoat, M.; Heine, T.; Banerjee, R. Interplaying Intrinsic and Extrinsic Proton Conductivities in Covalent Organic Frameworks. *Chem. Mater.* **2016**, *28*, 1489−1494.
(24) Xu, H.; Tao, S.; Jiang, D. Proton Conduction in Crystalline and Porous Covalent Organic frameworks. *Nat. Mater.* **2016**, *15*, 722−726.
(25) Cote, A. P.; Benin, A. I.; Ockwig, N. W.; O'Keeffe, M.; Matzger, A. J.; Yaghi, O. M. Porous, Crystalline, Covalent Organic Frameworks. *Science* **2005**, *310*, 1166−1170.
(26) Anoop Krishnan, K.; Anirudhan, T. S. Removal of Mercury(II) from Aqueous Solutions and Chlor-Alkali Industry Effluent by Steam Activated and Sulphurised Activated Carbons Prepared from Bagasse Pith: Kinetics and Equilibrium Studies. *J. Hazard. Mater.* **2002**, *92*, 161−183.
(27) Feng, W. G.; Borguet, E.; Vidic, R. D. Sulfurization of a Carbon Surface for Vapor Phase Mercury Removal - II: Sulfur forms and Mercury Uptake. *Carbon* **2006**, *44*, 2998−3004.
(28) Mercier, L.; Pinnavaia, T. I. Access in Mesoporous Materials: Advantages of a Uniform Pore Structure in the Design of a Heavy Metal Ion Adsorbent for Environmental Remediation. *Adv. Mater.* **1997**, *9* (6), 500.
(29) Aguila, B.; Sun, Q.; Perman, J. A.; Earl, L. D.; Abney, C. W.; Elzein, R.; Schlaf, R.; Ma, S. Efficient Mercury Capture Using Functionalized Porous Organic Polymer. *Adv. Mater.* **2017**, *29*, 1700665.
(30) Sun, Q.; Aguila, B.; Perman, J.; Earl, L. D.; Abney, C. W.; Cheng, Y.; Wei, H.; Nguyen, N.; Wojtas, L.; Ma, S. Postsynthetically Modified Covalent Organic Frameworks for Efficient and Effective Mercury Removal. *J. Am. Chem. Soc.* **2017**, *139*, 2786−2793.
(31) Bibby, A.; Mercier, L. Mercury (II) Ion Adsorption Behavior in Thiol-functionalized Mesoporous Silica Microspheres. *Chem. Mater.* **2002**, *14*, 1591.
(32) Wu, Z.; Zhao, D. Ordered Mesoporous Materials as Adsorbents. *Chem. Commun.* **2011**, *47*, 3332.
(33) Shenashen, M. A.; El-Safty, S. A.; Elshehy, E. A. Architecture of Optical Sensor for Recognition of Multiple Toxic Metal Ions From Water. *J. Hazard. Mater.* **2013**, *260*, 833−843.
(34) Khajeh, M.; Laurent, S.; Dastafkan, K. Nanoadsorbents: Classification, Preparation, and Applications (With Emphasis on Aqueous Media). *Chem. Rev.* **2013**, *113*, 7728.
(35) Dave, N.; Chan, M. Y.; Huang, P. J. J.; Smith, B. D.; Liu, J. Regenerable DNA-Functionalized Hydrogels for Ultrasensitive, Instrument-free Mercury (II) Detection and Removal in Water. *J. Am. Chem. Soc.* **2010**, *132*, 12668.
(36) Esser-Kahn, A. P.; Iavarone, A. T.; Francis, M. B. Metal-lothionein-cross-linked Hydrogels for the Selective Removal of Heavy Metals from Water. *J. Am. Chem. Soc.* **2008**, *130*, 15820.
(37) Kabiri, S.; Tran, D. N. H.; Cole, M. A.; Losic, D. Functionalized Three-dimensional (3D) Graphene Composite for High Efficiency Removal of Mercury. *Environ. Sci.: Water Res. Technol.* **2016**, *2*, 390−402.
(38) Li, R.; Liu, L.; Yang, F. Preparation of Polyaniline/Reduced Graphene Oxide Nanocomposite and Its Application in Adsorption of Aqueous Hg (II). *Chem. Eng. J.* **2013**, *229*, 460−468.
(39) Abney, C. W.; Gilhula, J. C.; Lu, K.; Lin, W. Metal Organic Framework Templated Inorganic Sorbents for Rapid and Efficient Extraction of Heavy Metals. *Adv. Mater.* **2014**, *26*, 7993.
(40) Fang, Q. R.; Yuan, D. Q.; Sculley, J.; Li, J. R.; Han, Z. B.; Zhou, H. C. Functional Mesoporous Metal-organic Frameworks for the Capture of Heavy Metal Ions and Size-selective Catalysis. *Inorg. Chem.* **2010**, *49*, 11637.
(41) Xie, L.; Yu, Z.; Islam, S. M.; Shi, K.; Cheng, Y.; Yuan, M.; Zhao, J.; Sun, G.; Li, H.; Ma, S.; Kanatzidis, M. G. Remarkable Acid Stability of Polypyrrole-MoS_4A Highly Selective and Efficient Scavenger of Heavy Metals Over a Wide pH Range. *Adv. Funct. Mater.* **2018**, *28*, 1800502.
(42) Haitzer, M.; Aiken, G. R.; Ryan, J. N. Binding of Mercury (II) to Aquatic Humic Substances: Influence of pH and Source of Humic Substances. *Environ. Sci. Technol.* **2003**, *37*, 2436−2441.
(43) Zhu, X.; Alexandratos, S. D. Polystyrene-supported Amines: Affinity for Mercury (II) as a Function of the Pendant Groups and the Hg (II) Counterion. *Ind. Eng. Chem. Res.* **2005**, *44*, 8605−8610.
(44) Pearson, R. G. Hard and Soft Acids and Bases. *J. Am. Chem. Soc.* **1963**, *85*, 3533.
(45) Geng, B. Y.; Wang, H. Y.; Wu, S.; Ru, J.; Tong, C. C.; Chen, Y. F.; Liu, H. Z.; Wu, S. C.; Liu, X. Y. Surface-Tailored Nanocellulose Aerogels with Thiol-Functional Moieties for Highly Efficient and Selective Removal of Hg(II) Ions from Water. *ACS Sustainable Chem. Eng.* **2017**, *5*, 11715−11726.
(46) Ding, S.-Y.; Dong, M.; Wang, Y.-W.; Chen, Y.-T.; Wang, H.-Z.; Su, C.-Y.; Wang, W. Thioether-based Fluorescent Covalent Organic Framework for Selective Detection and Facile Removal of Mercury (II). *J. Am. Chem. Soc.* **2016**, *138*, 3031.
(47) Palkovits, R.; Antonietti, M.; Kuhn, P.; Thomas, A.; Schüth, F. Solid Catalysts for the Selective Low-Temperature Oxidation of Methane to Methanol. *Angew. Chem., Int. Ed.* **2009**, *48*, 6909−6912.
(48) Talapaneni, S. N.; Hwang, T. H.; Je, S. H.; Buyukcakir, O.; Choi, J. W.; Coskun, A. Elemental-Sulfur-Mediated Facile Synthesis of

DOI: 10.1021/acssuschemeng.9b00567
ACS Sustainable Chem. Eng. 2019, 7, 7353−7361

a Covalent Triazine Framework for High-Performance Lithium-Sulfur Batteries. *Angew. Chem., Int. Ed.* **2016**, *55*, 3106−3111.
(49) Puthiaraj, P.; Lee, Y. R.; Zhang, S.; Ahn, W. S. Triazine-based Covalent Organic Polymers: Design, Synthesis and Applications in Heterogeneous Catalysis. *J. Mater. Chem. A* **2016**, *4*, 16288−16311.
(50) Kuhn, P.; Antonietti, M.; Thomas, A. Porous, Covalent Triazine Based Frameworks Prepared by Ionothermal Synthesis. *Angew. Chem., Int. Ed.* **2008**, *47*, 3450−3453.
(51) Kuhn, P.; Thomas, A.; Antonietti, M. Toward Tailorable Porous Organic Polymer Networks: A High-temperature Dynamic Polymerization Scheme Based on Aromatic Nitriles. *Macromolecules* **2009**, *42*, 319−326.
(52) Bhunia, A.; Vasylyeva, V.; Janiak, C. From a Supramolecular Tetranitrile to A Porous Covalent Triazine-based Framework with High Gas Uptake Capacities. *Chem. Commun.* **2013**, *49*, 3961−3963.
(53) Hanif, Z.; Lee, S.; Qasim, G. H.; Ardiningsih, I.; Kim, J. A.; Seon, J.; Han, S.; Hong, S.; Yoon, M. H. Polypyrrole Multilayer-Laminated Cellulose for Large-Scale Repeatable Mercury Ion Removal. *J. Mater. Chem. A* **2016**, *4*, 12425−12433.
(54) Buyukcakir, O.; Je, S. H.; Talapaneni, S. N.; Kim, D.; Coskun, A. Charged Covalent Triazine Frameworks for CO_2 Capture and Conversion. *ACS Appl. Mater. Interfaces* **2017**, *9*, 7209−7216.
(55) Wang, K.; Huang, H.; Liu, D.; Wang, C.; Li, J.; Zhong, C. Covalent Triazine-Based Frameworks with Ultramicropores and High Nitrogen Contents for Highly Selective CO_2 Capture. *Environ. Sci. Technol.* **2016**, *50*, 4869−4876.
(56) Huang, N.; Zhai, L.; Xu, H.; Jiang, D. Stable Covalent Organic Frameworks for Exceptional Mercury Removal from Aqueous Solutions. *J. Am. Chem. Soc.* **2017**, *139*, 2428−2434.
(57) Ho, Y. S.; McKay, G. Sorption of Dye from Aqueous Solution by Peat. *Chem. Eng. J.* **1998**, *70*, 115−124.
(58) Ahmed, S.; Brockgreitens, J.; Xu, K.; Abbas, A. A Nanoselenium Sponge for Instantaneous Mercury Removal to Undetectable Levels. *Adv. Funct. Mater.* **2017**, *27*, 1606572.
(59) Huang, L.; He, M.; Chen, B.; Cheng, Q.; Hu, B. Highly Efficient Magnetic Nitrogen-Doped Porous Carbon Prepared by One-Step Carbonization Strategy for Hg^{2+} Removal from Water. *ACS Appl. Mater. Interfaces* **2017**, *9*, 2550−2559.
(60) Li, B.; Zhang, Y.; Ma, D.; Shi, Z.; Ma, S. Mercury Nano-trap for Effective and Efficient Removal of Mercury (II) from Aqueous Solution. *Nat. Commun.* **2014**, *5*, 5537.
(61) Ding, L.; Luo, X.; Shao, P.; Yang, J.; Sun, D. Thiol-Functionalized Zr-Based Metal-Organic Framework for Capture of Hg(II) through a Proton Exchange Reaction. *ACS Sustainable Chem. Eng.* **2018**, *6*, 8494−8502.
(62) Manos, M. J.; Petkov, V. G.; Kanatzidis, M. G. $H_{2x}M_{nx}Sn_{3-x}S_6$ (x = 0.11−0.25): A Novel Reusable Sorbent for Highly Specific Mercury Capture Under Extreme pH Conditions. *Adv. Funct. Mater.* **2009**, *19*, 1087−1092.
(63) Weber, W. J.; Morris, J. C. Kinetics of adsorption on carbon from solutions. *J. Sanit. Eng. Div. Am. Soc. Civ. Eng.* **1963**, *89*, 31−60.
(64) Fierro, V.; Torné-Fernández, V.; Montané, D.; Celzard, A. Adsorption of Phenol onto Activated Carbons Having Different Textural and Surface Properties. *Microporous Mesoporous Mater.* **2008**, *111*, 276.

NOTE ADDED AFTER ASAP PUBLICATION

Due to a production error, this paper was published ASAP on March 21, 2019, with an error in the Experimental Section. The corrected version was reposted on April 1, 2019.

DOI: 10.1021/acssuschemeng.9b00567
ACS Sustainable Chem. Eng. 2019, 7, 7353−7361